Computational Materials Science 153 (2018) 326–337

Contents lists available at ScienceDirect

Computational Materials Science

journal homepage: www.elsevier.com/locate/commatsci

An in-depth investigation of Mg-Zn-Ca metallic glasses: A first principles study

Mustafa Erkartal, Murat Durandurdu*

Abdullah Gül University, Materials Science & Nanotechnology Engineering, Kayseri, Turkey

ARTICLE INFO

Keywords:
Metallic glass
Ab-initio
Amorphous
Mechanical properties

ABSTRACT

The atomic structures, glass forming evolutions, mechanical properties and high pressure behavior of $Mg_{75}Zn_{20}Ca_5$ and $Mg_{60}Zn_{35}Ca_5$ bulk metallic glasses, which are promising candidates for biomedical implants, have been examined by using ab initio molecular dynamics simulations. The pair-distribution function and coordination number analyses show that increasing Zn content in the alloy results in a decrease in several bond distances and an increase in the total coordination number of each species due to the atomic size difference between Mg and Zn atoms. According to the Voronoi tessellation, bond pair and bond angle distribution analyzes, the fivefold geometrical arrangements (pentagonal-bipyramid) are the most predominant in the first coordination shell, indicating the stability of the amorphous states and their dense atomic packing. The most striking result emerged from the calculations of mechanical properties is that an increase of Zn ($\geq$30%) content in the alloy yields embrittlement in the alloys. Under uniaxial compressions, both compositions undergo structural failure between 6 and 8 GPa. Under hydrostatic pressure, a diminishing in fcc/hcp ordering and an enlargement of the ideal icosahedral ordering may indicate a more disordered structure. In our view, these results represent a good step toward understanding the atomic structures Mg-Zn-Ca bulk metallic glasses.

1. Introduction

Bulk metallic glasses (BMGs) have been attracting widespread interests due to their outstanding mechanical, physical and chemical properties [1–3]. A beneficial feature of BMGs is their amorphous structure, which offers several important characteristics, for instance higher mechanical strengths in the absence of dislocation defects and tunable macroscopic properties by a wide range of chemical compositions [3,4]. Mg-Zn-Ca BMGs have many unique properties as compared to other metallic glasses. Firstly, Mg, Zn and Ca are biocompatible elements because they are normally found in human body and are therefore suitable for biomedical applications. These types of BMGs also have very low Young's and shear moduli, making them a promising candidate for implants in orthopedic applications. While most metal prostheses used as implants require removal by a second operation from the body, Mg-Zn-Ca BMGs degrade/corrode in the body by the effects of body fluids and thus no additional operation is needed. In addition, since the elemental metals forming these BMGs are also found in the bone, they also contribute to the healing process [5–14]. Yet there are several challenges that are still needed to overcome for their practical applications. One of them is the rapid corrosion of these BMGs, which weakens the mechanical strength of implants before the complete recovery. Another problem, perhaps the most important, is that when Mg corrodes under the body fluids, hydrogen gas, which is very harmful for tissues and organs, is released (Corrosion reaction of Mg: $Mg + 2H_2O \rightarrow Mg^{2+} + 2OH^- + H_2$) [7,12,13]). Recently, Zyberg et al. [7] have shown in their groundbreaking study that releasing of hydrogen gas can be reduced and even completely eliminated by the formation of Zn-rich and O-rich passivating layer on alloy surfaces. Thus, the slower degradation of BMGs can be achievable, and plus their mechanical properties can be preservable during the healing. The formation of this passivating layer does indeed depend on the amount of Zn (at least 28%) and the short-range order of the glasses [7]. Therefore, understanding the short-range order of these amorphous materials is mandatory to control and adjust many macroscopic properties such as corrosion rate, mechanical properties etc.

Although Mg-Zn-Ca glasses are very promising materials and have attracted substantial interests, there are very few publications on theoretical modeling and investigations of their structure at the atomistic level. Preliminary investigations focused on mainly binary alloys such as Mg-Zn [15], Mg-Ca [16], and it was showed that their local structure was dominated by icosahedral motifs. In the first study on Mg-Zn-Ca ternary alloys, their structural properties were investigated using an empirical tight-binding potential [17]. In another study, Gulenko et al.

* Corresponding author.
E-mail address: murat.durandurdu@agu.edu.tr (M. Durandurdu).

https://doi.org/10.1016/j.commatsci.2018.07.013
Received 5 April 2018; Received in revised form 5 July 2018; Accepted 6 July 2018
Available online 10 July 2018
0927-0256/

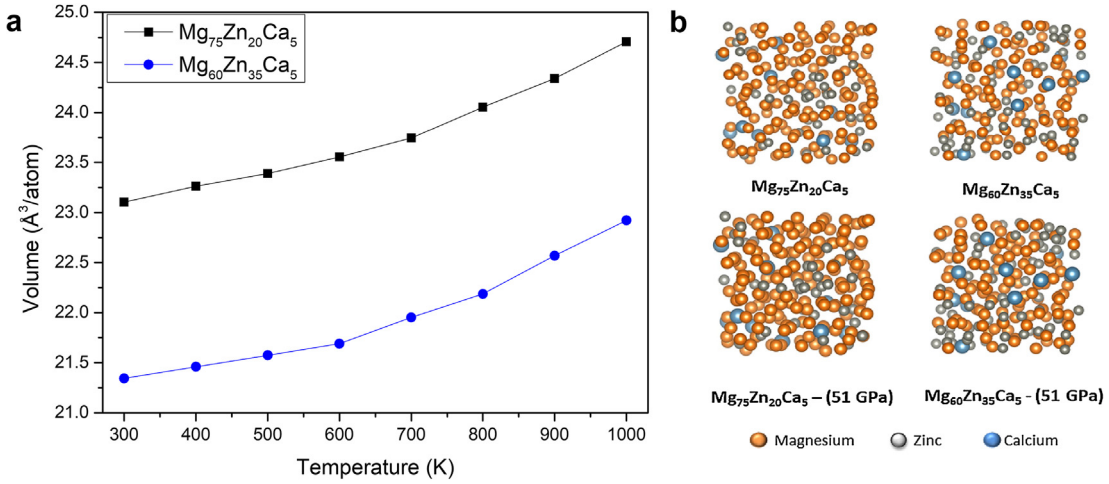

Fig. 1. (a) Variation of volume per atom as a function of temperature during the quenching processes (b) The view of simulated systems.

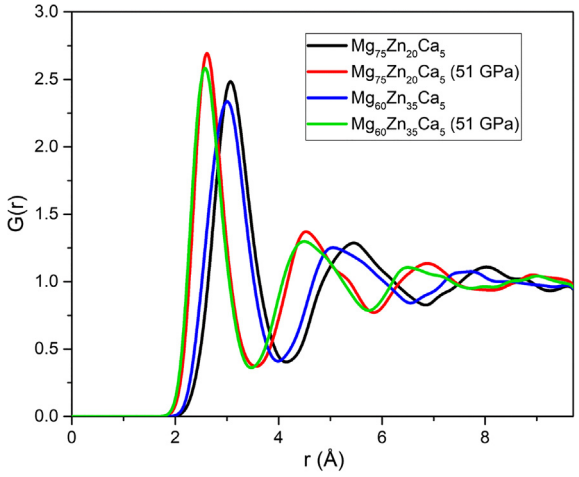

Fig. 2. Total pair distribution functions (PDFs) of the glasses.

[18] simulated Mg-Zn-Ca alloys having different compositions using a classical molecular dynamics (MD) technique. Although these simulation techniques allow working on large systems with too many atoms, their results are highly dependent on the force field used. Additionally many quantum mechanical phenomena (such as bonding, charge transfer) are ignored during these calculations. In contrast, quantum mechanical simulations based ab initio molecular dynamics (AIMD) techniques yield more accurate results, though it lets modeling of fewer atoms [19]. To the best of our knowledge, there are four detailed reports on AIMD simulations of Mg-Zn-Ca ternary alloys in the literature. Zhao et al. [20] calculated the viscosities of alloys in liquid form and correlated the well glass forming ability (GFA) of these alloys with sluggish mobility of atoms. Mahjoub et al. [21] examined the electronic and elastic properties of Mg-Zn-Ca alloys with different compositions. Li et al. [22] reported that a percolated Zn-Zn networks could form with an increase in Zn content, which also affected the corrosion performance of these glasses. Christie studied Mg-Zn-Ca BMGs with two different compositions and observed a moderate avoidance of Zn-Zn bonding [11].

In this study, the structural and mechanical properties of Mg-Zn-Ca alloys in two different compositions, one of which had been simulated previously [11], was investigated by using an AIMD simulation. For both compositions, pair distribution functions (PDFs), the Voronoi polyhedrons (VPs), coordination number (CN) and bond pair (BP) analyses were performed. In the light of obtained results, the short-range order (SRO) and glass forming ability (GFA) of the glasses were explored. Additionally, the structural changes in both compositions under hydrostatic and uniaxial stresses and their elastic properties were investigated. We believe that our results may improve our knowledge about Mg-based BMGs and be a good guide for optimizing the composition and mechanical properties of glasses for desired applications.

2. Methodology

The alloys with $Mg_{75}Zn_{20}Ca_5$ and $Mg_{60}Zn_{35}Ca_5$ compositions were chosen for this work. The AIMD calculations were performed by using the SIESTA ab initio simulation code [23]. The Troulier-Martins pseudopotentials [24] for definition of the ion-electron interactions and the Perdew-Burke-Ernzerhof (PBE) generalized gradient approximation were used for the calculation of exchange-correlation energy [25]. The double-ζ polarized orbitals were preferred for the calculations. The mesh cut-off was set to 150 Ry and only Γ-point sampling of k-mesh was used. The time step in the AIMD simulations was chosen as 1 fs (fs). Each simulation box consisted of 200 atoms with periodic boundary conditions. The initial configuration of the simulation boxes was randomly built using a hard-sphere model. The starting structures were held at 1000 K for 80 picoseconds to obtain well equilibrated liquid states, and then the liquid-states were gradually quenched to 300 K with 100 K temperature step in wholly 140 ps. All of these simulations were carried out within the NPT (constant number of atoms, constant pressure, and constant temperature) ensemble. After that, the structures at 300 K were relaxed by using a conjugate gradient (CG) approach and a variable cell optimization method in which the simulation box's shape and size and the atomic coordinates were permitted to adjust with 0.01 eV/Å force and 0.25 GPa stress tolerances. All structural and mechanical calculations were performed by using these optimized configurations unless otherwise stated. The high-pressurized forms of both alloys were achieved by using the variable cell optimization method with a gradual increase of pressure up to 51 GPa. A uniaxial stress was employed along one direction while the other stress components were firstly set to zero, and the simulation vectors were allowed to amend to the applied stress. This process was repeated for all three directions. For both hydrostatic and uniaxial stress applications, to have a continuous stress path, the initial lattice parameters and atomic coordinates at each stress step were gotten from the optimized lattice parameters and coordinates of prior step. The VESTA program for visualization of the

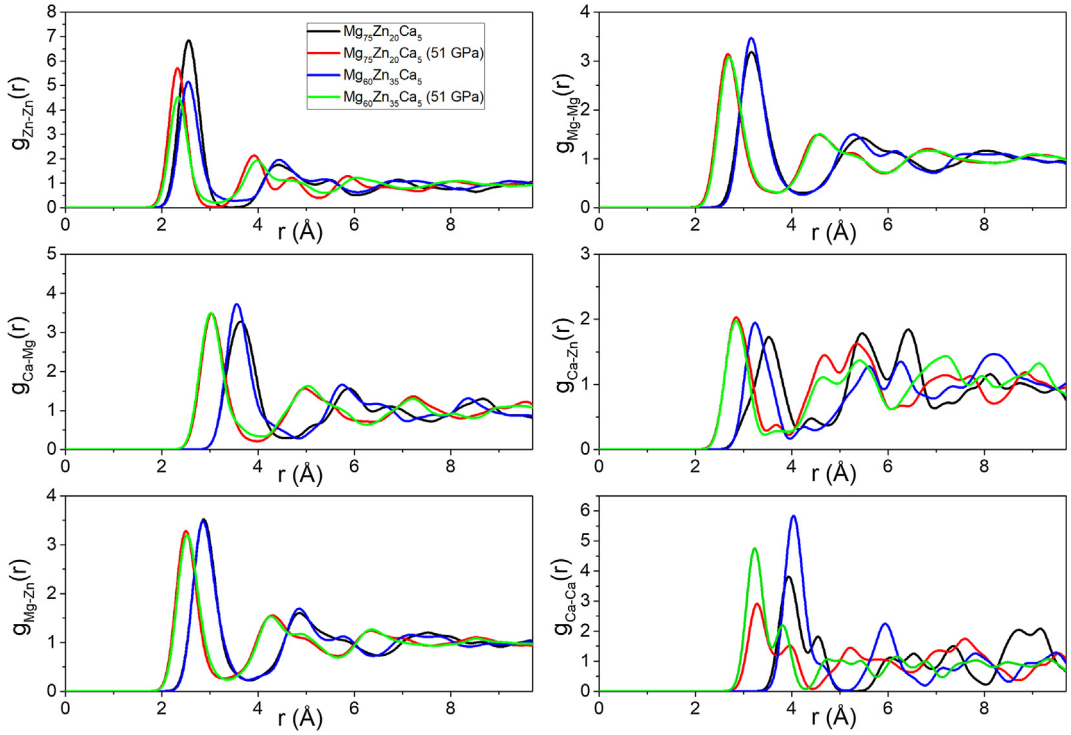

Fig. 3. Partial pair distribution functions of the glasses.

Table 1
Interatomic bond distances r_{ij} (Å).

Species	Mg-Mg	Zn-Zn	Ca-Ca	Ca-Mg	Ca-Zn	Zn-Mg	Ref.
$Mg_{75}Zn_{20}Ca_5$	3.15	2.55	3.92	3.55	3.26	2.87	This work
$Mg_{75}Zn_{20}Ca_5$ (51 GPa)	2.67	2.32	3.28	3.03	2.84	2.50	This work
$Mg_{60}Zn_{35}Ca_5$	3.16	2.55	3.92	3.51	3.18	2.85	This work
$Mg_{60}Zn_{20}Ca_5$ (51 GPa)	2.70	2.34	3.23	3.02	2.84	2.52	This work
$Mg_{72}Zn_{23}Ca_5$ (ref-Ch)	3.00	2.55	4.10	3.35	3.05	2.75	[11]
$Mg_{60}Zn_{20}Ca_5$ (ref-Ch)	3.05	2.60	3.95	3.40	3.05	2.80	[11]
$Mg_{74}Zn_{21}Ca_5$ (ref-li)	3.15	2.58	–	3.48	3.16	2.83	[22]
$Mg_{62}Zn_{33}Ca_5$ (ref-li)	3.15	2.62	–	3.48	3.20	2.84	[22]
$Mg_{72}Zn_{28}$	3.22	2.79	–	–	–	2.98	[28]
$Mg_{90}Ca_{10}$	3.18	–	4.05	3.67	–	–	[16]
$r_{metallic}$	3.20	2.68	3.94	3.57	3.31	2.94	[29]
$r_{covalent}$	2.82	2.44	3.52	3.17	2.98	2.63	[29]

obtained structures was used [26].

3. Results

Fig. 1a presents the variation of volume per atom as a function of temperature. Clearly, the volume decreases gradually during the quenching. Yet there is a change in slope for both compositions, allowing us to roughly guess the glass-transition temperature (T_g). It can be suggested that T_g is between 700 and 800 K for $Mg_{75}Zn_{20}Ca_5$, and is between 600 and 700 K for $Mg_{60}Zn_{35}Ca_5$. The view of relaxed structures for both compositions and their high-pressurized forms are illustrated in Fig. 1b.

3.1. PDFs

Pair distribution function (PDF) is one of powerful methods to investigate the structural arrangement of materials. The partial PDF is expressed by,

$$g_{\alpha\beta}(r) = \frac{N}{4\pi r^2 \rho N_\alpha N_\beta} \sum_{i=1}^{N_\alpha} \sum_{j=1}^{N_\beta} \delta(r - |\vec{r}_{ij}|) \quad (1)$$

where N, N_α, N_β, ρ are total number of atoms, number of α atoms, number of β atoms used in the simulation and the density of simulation box, respectively. The total PDF is defined by,

$$g(r) = \sum_{\alpha,\beta} c_\alpha c_\beta Z_\alpha Z_\beta g_{\alpha\beta}(r) \Big/ \left(\sum_\alpha c_\alpha Z_\alpha \right)^2 \quad (2)$$

where Z and c are the atomic number of species α, β and compositions in the calculations, respectively.

Figs. 2 and 3 show the calculated total and partial PDFs of two different BMGs compositions. As can be seen from Fig. 2, the position of the total PDF peaks slightly shifts to lower r values with increasing Zn content in the BMGs, indicating a decrease of interatomic distances, especially in Mg-Ca, Zn-Ca, and Zn-Mg (Fig. 3 and Table 1). This is in good agreement with the previous findings [11,22] and can be explained by the fact that Zn atom has a smaller size than Mg. Furthermore, the shoulder peak between 4 and 6 Å points out the existence of a medium range order (MRO), however an in depth-investigation of MRO needs a large supercell with thousands atoms, and yet it is an onerous task with today's ab initio methods.

As shown in Fig. 3, the Ca-centered partial PDF exhibits considerably large fluctuations at distances beyond 6 Å. These variations can be assigned to statistical noise which originates from a low concentration of Ca atoms in the given compositions [11].

To explore the structural evolution of the ternary glasses during the

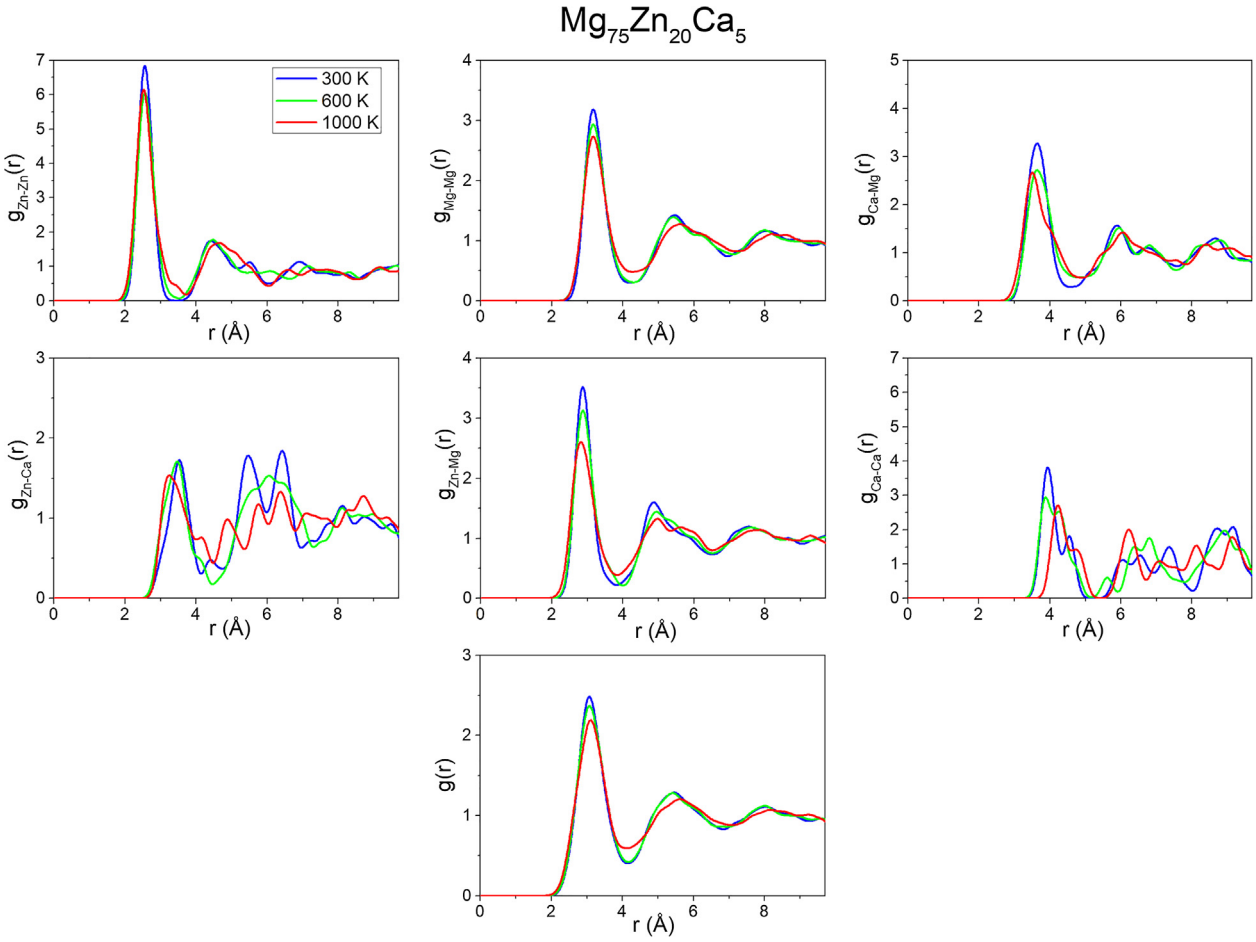

Fig. 4. Total and partial pair distribution functions as a function of temperature for $Mg_{75}Zn_{20}Ca_5$.

melt-quenching process, partial PDFs for both compositions as a function of temperature are shown in Figs. 4 and 5. When the external temperature is reduced from the equilibrium liquid phase (1000 K) to the amorphous solid state at room temperature (300 K), the first peak of all partial and total PDFs gets sharper and more intense due to the development of more ordered arrangements. The intensity of first peak of $g_{Mg\text{-}Mg}(r)$, $g_{Zn\text{-}Mg}(r)$ and $g_{Ca\text{-}Mg}(r)$ in $Mg_{75}Zn_{20}Ca_5$ and $g_{Zn\text{-}Zn}(r)$, $g_{Mg\text{-}Mg}(r)$, $g_{Zn\text{-}Ca}(r)$ in $Mg_{60}Zn_{35}Ca_5$ increases significantly with decreasing temperature as compared with other pairs in both compositions. These observations suggest that Mg-Mg, Zn-Mg and Ca-Mg are favorable neighboring in $Mg_{75}Zn_{20}Ca_5$ while Zn-Zn, Mg-Mg and Zn-Ca are preferred ones in $Mg_{60}Zn_{35}Ca_5$ [22].

3.2. Bonds

Table 1 lists the bond lengths derived from the first maxima of the partial PDFs for compositions and their high-pressurized structures, as well as metallic and covalent bonds lengths from the literature. The estimated bond lengths are in a range between covalent and metallic bonds but they are smaller than as compared to bond lengths in binary alloys of the same constitutes. It may be claimed that negative enthalpy of constituents [27] and the reduced available space due to incorporation of relatively larger Ca atoms are responsible for a bond shortening [18].

3.3. Voronoi analysis and coordination numbers

Voronoi tessellation analysis is a versatile method that provides significant information on local order and can be used to determine total and partial CNs [30,31]. In this method, for a given atom, a Voronoi polyhedron is formed by the region covered by only the nearest neighbors of that atom. Each polyhedron is defined by a signature, $\langle \nu_3,\nu_4,\nu_5,\nu_6 \ldots \rangle$ where ν_m addresses to the number of m-edged faces on a Voronoi polyhedron. Also, the number of faces of the Voronoi polyhedra is equal to coordination number as $CN = \sum \nu_m$ [32,33].

The distribution of total and partial CNs determined from the Voronoi analysis for both compositions and their high-pressurized forms are shown in Fig. 6. These results reveal that CNs are quite sensitive to composition. When the content of Zn atoms increases, the total CN for each species increases as follows: from 13.09 to 13.67 (4.4%) for Mg, from 10.65 to 10.97 (3.0%) for Zn, and from 16.00 to 17.00 (6.3%) for Ca.

We note from Table 2 that the partial CNs of both Mg and Zn atoms increase with increasing Zn content in the glasses. This can be explained by the atomic size difference between Mg and Zn atoms. The relatively smaller size of Zn atoms allows the cluster-centered atoms to coordinate with more atoms, resulting in an increase in the CNs [34]. In fact, as can be seen from partial CNs and the VPs, Zn atoms are mostly surrounded by Mg atom.

Fig. 7 shows the distribution of the most abundant types of Mg-, Zn-,

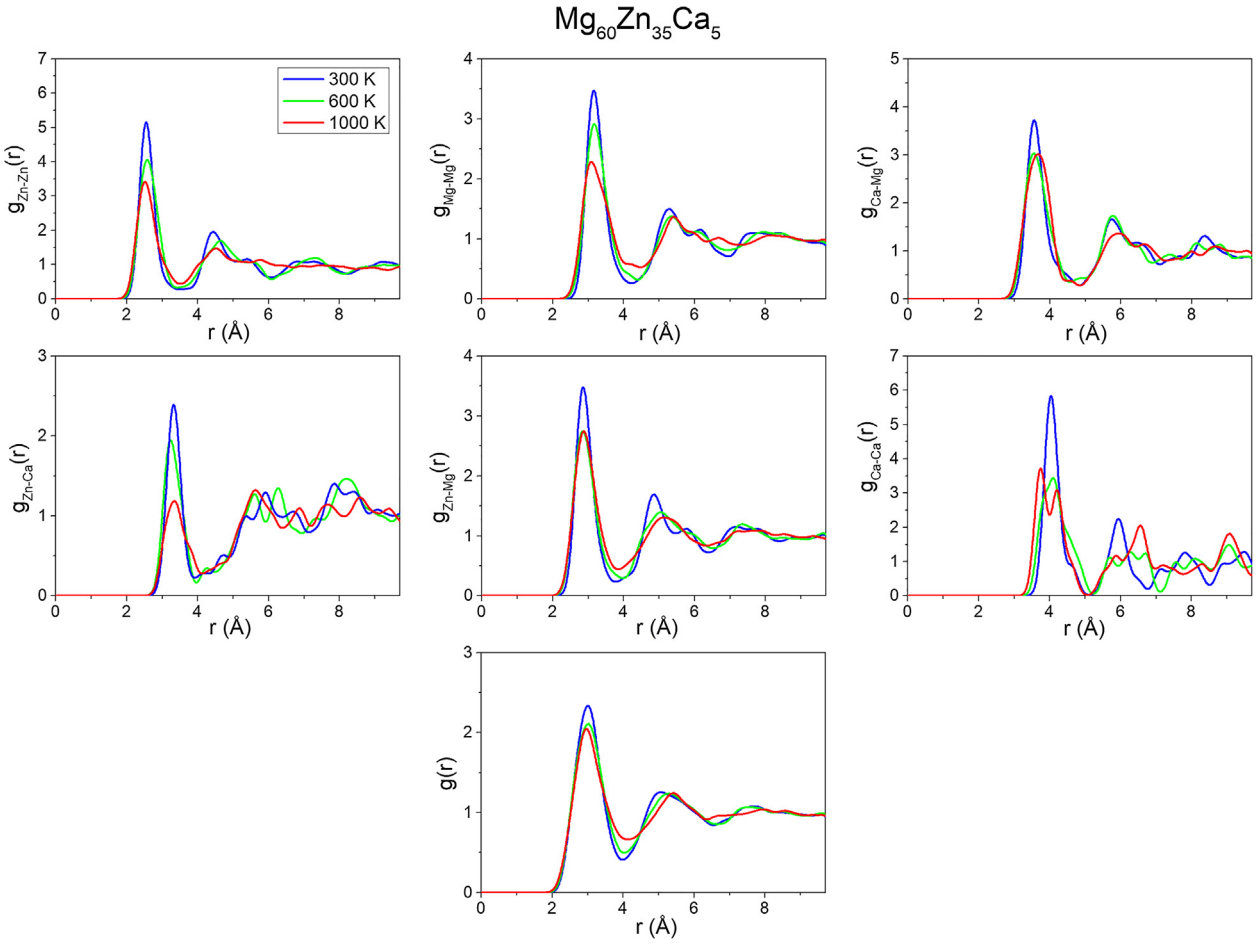

Fig. 5. Total and partial pair distribution functions as a function of temperature for $Mg_{60}Zn_{35}Ca_5$.

and Ca-centered VPs. Depending on the central atom, the distribution of the dominant VPs are as follows: For Mg-centered clusters, the percentage of ⟨0,2,8,4⟩, ⟨0,3,6,4⟩, ⟨0,1,10,2⟩, and ⟨0,0,12,0⟩ VPs is 7–8%, 8–9%, 11–15% and 9–15%, respectively. As can be seen, none of these VPs is a dominant percentage of the others. For Zn-centered clusters, on the other hand, the fraction of ⟨0,0,12,0⟩, ⟨0,2,8,0⟩, ⟨0,2,8,1⟩, ⟨0,3,6,0⟩ VPs is 26–28%, 20%, 10–18%, 10–18%, correspondingly. Here the ⟨0,0,12,0⟩ and ⟨0,2,8,0⟩, ⟨0,2,8,1⟩ indices represent icosahedral and icosahedral-like configurations [30], and the percentage of these structures is more than 60%. Based on this fact, it can be suggested that Zn-centered clusters prefer to form icosahedral ordering. These results are also correlated with the CN analysis. Since the mean CN of Mg and Ca is higher than 12, the ideal icosahedral motif is not predominant in such clusters whereas icosahedral and/or icosahedral-like motifs can dominate in Zn-centered clusters due to the CN equal to 12 or less than 12. Note that defining a dominant type of VPs for Ca-centered cluster is not possible due to a low content of this species in the alloys.

We also investigate the evolution of VPs during the liquid-solid transition. The VPs that show drastic alterations are given in Fig. 8. For Zn-centered clusters, the most dramatic change is found in ⟨0,0,12,0⟩ with around 20% increase throughout the liquid-solid transition in both alloys. Similarly, for Mg-centered clusters, the remarkable change is observed in ⟨0,0,12,0⟩ with about 10% increase. This may be attributed to the importance of icosahedral motifs in amorphous solids.

Importantly, the most conspicuous observation emerged from the Voronoi analysis is, regardless of the atomic species, the dominance of 5-fold geometry, indicating the pentagonal-bipyramid arrangements of atoms [35,36]. This observation is particularly crucial because the stability of metallic amorphous structures is commonly attributed to the 5-fold geometrical arrangements [36]. It is also suggested that the ⟨0,0,12,0⟩ type of cluster is a barrier that obstructs to the crystallization [27].

3.4. Bond-pair analysis

The BP analysis, a method proposed by Honeycutt and Andersen [37], is carried out to describe the local environment and structural evolution of the glass during liquid-solid transition and high pressure. In this method, the atomic local circumstances are represented with a 4-digit shorthand, indexing i,j,k, and l integers. The first index (i), either 1 or 2, imply that whether two atoms are termed as a bond pair (i = 1) or not (i = 2). The second index (j), denotes number of common near-neighbors shared by the root pair. The third index (k) stands for the number of bonds among the neighbors. Since these three indexes are inadequate to describe a unique BP, the fourth index (l) is used [37]. As stated by this shorthand, the 1431, 1541 and 1551 indices denote the icosahedral ordering; 1441 and 1661 indices represent body-centered cubic (bcc) ordering, 1421 and 1422 indices represent face-centered cubic (fcc) and hexagonal closed pack (hcp) ordering; and 1311 and

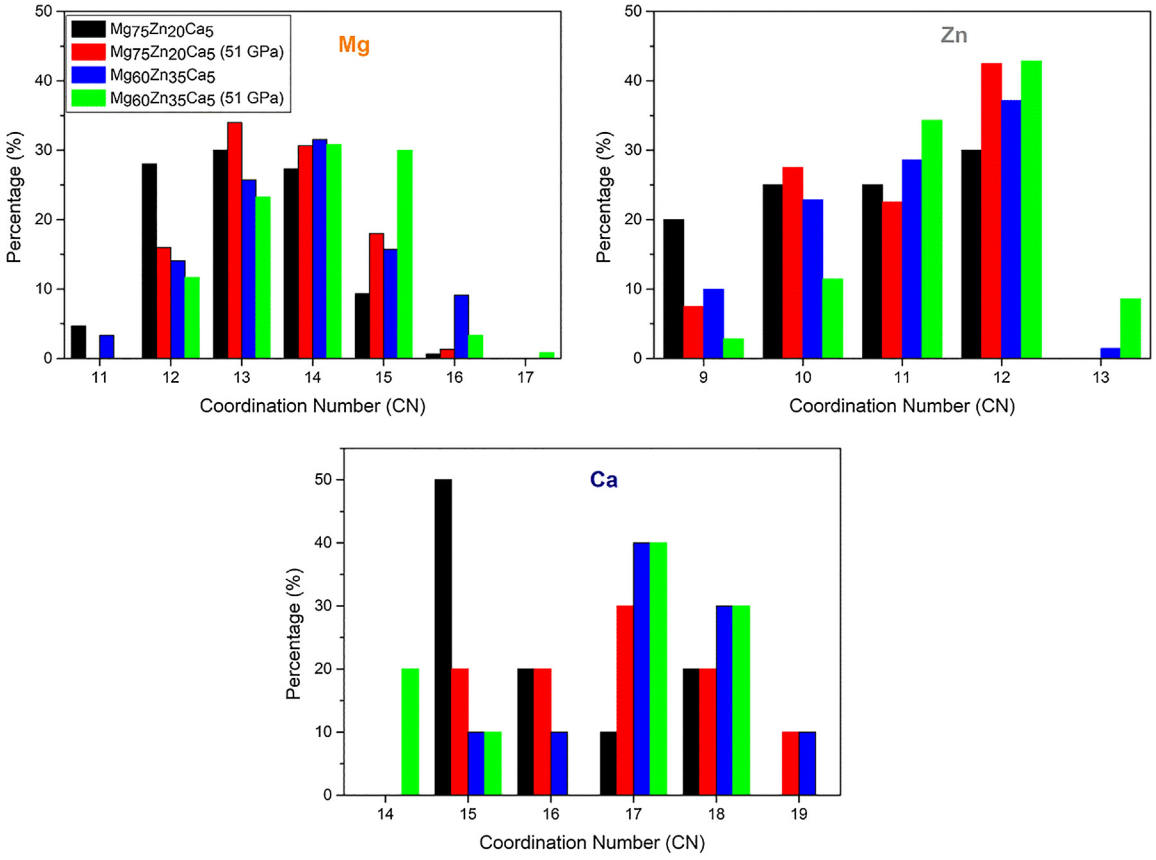

Fig. 6. Distributions of Mg-, Zn-, and Ca-centered clusters by their total coordination numbers (CNs).

Table 2
Average partial coordination numbers calculated by Voronoi polyhedra.

Composition	Mg-Mg	Mg-Zn	Mg-Ca	Mg total
$Mg_{75}Zn_{20}Ca_5$	10.15	2.05	0.89	13.09
$Mg_{75}Zn_{20}Ca_5$ (51 GPa)	10.41	2.13	0.94	13.48
$Mg_{60}Zn_{35}Ca_5$	8.77	3.85	1.05	13.67
$Mg_{60}Zn_{35}Ca_5$ (51 GPa)	8.78	4.05	1.02	13.85
Composition	**Zn-Mg**	**Zn-Zn**	**Zn-Ca**	**Zn total**
$Mg_{75}Zn_{20}Ca_5$	7.68	2.55	0.42	10.65
$Mg_{75}Zn_{20}Ca_5$ (51 GPa)	7.98	2.55	0.47	11.00
$Mg_{60}Zn_{35}Ca_5$	6.60	3.97	0.40	10.97
$Mg_{60}Zn_{35}Ca_5$ (51 GPa)	6.94	4.06	0.43	11.43
Composition	**Ca-Mg**	**Ca-Zn**	**Ca-Ca**	**Ca total**
$Mg_{75}Zn_{20}Ca_5$	13.50	1.70	0.80	16.00
$Mg_{75}Zn_{20}Ca_5$ (51 GPa)	14.10	1.90	0.80	16.80
$Mg_{60}Zn_{35}Ca_5$	12.60	2.80	1.60	17.00
$Mg_{60}Zn_{35}Ca_5$ (51 GPa)	12.30	3.00	1.00	16.30

1321 correspond to disordered atomic arrangements [37–39].

Fig. 9(a) shows the distribution of BPs with compositions and pressures. Along with slight differences among the compositions, for both compositions the summation of BPs ratio attributed to icosahedral ordering (i.e. 1551) and distorted icosahedral ordering (i.e. 1431 and 1541) are overwhelming majority, around 77%. The distribution of other BPs is slightly dependent on composition. Accordingly, the percentages of 1441 and 1661 are 2.3% and 5.0%, respectively, for $Mg_{75}Zn_{20}Ca_5$, whereas they are 3.6% and 7.1% for $Mg_{60}Zn_{35}Ca_5$. Similarly, the percentages of 1421 and 1422 are 3.3% and 6.7% correspondingly for $Mg_{75}Zn_{20}Ca_5$, while they are 2.0% and 5.7% for $Mg_{60}Zn_{35}Ca_5$.

We investigate the BP evolution as a function of temperature for both compositions. As shown in Fig. 9(b and c), both alloys have similar trend. When the temperature is decreased from 1000 K to 300 K, the percentage of 1431, 1541 and 1551 increases an amount of ~25%. Conversely, the fraction of 1441 and 1661 type of BP drops with an amount of ~40% throughout liquid-solid transition. In addition, the ratio of disordering type of BPs (1311, 1321) converges to zero as the temperature decreases from 1000 K to 300 K. According to the whole results, the obtained glass structures consist of imperfect ordered and amorphous structures.

3.5. Bond-angle distribution

To provide further information on local chemical structure, bond angle distributions were analyzed. The bond angle distribution function $f(\theta)$ defines the probability that the directions from a central atom to two of its neighbors form an angle θ. Indeed, $f(\theta)$ is a radial average over triplet correlation function $g(R_1, R_2, \theta)$ over the nearest neighbor coordination shell:

$$f(\theta) = 16\pi^2 \int_0^{d_1} \int_0^{d_1} R_1^2 R_2^2 g(R_1) g(R_2) g_3(R_1, R_2, \theta) dR_1 dR_2 \quad (3)$$

where d_1 is the maximum distance between two neighbor atom. [40] Fig. 10 shows the Mg-X-Mg and Zn-X-Zn bond angle distributions for both alloys and their pressurized form. The characteristic first peak (α)

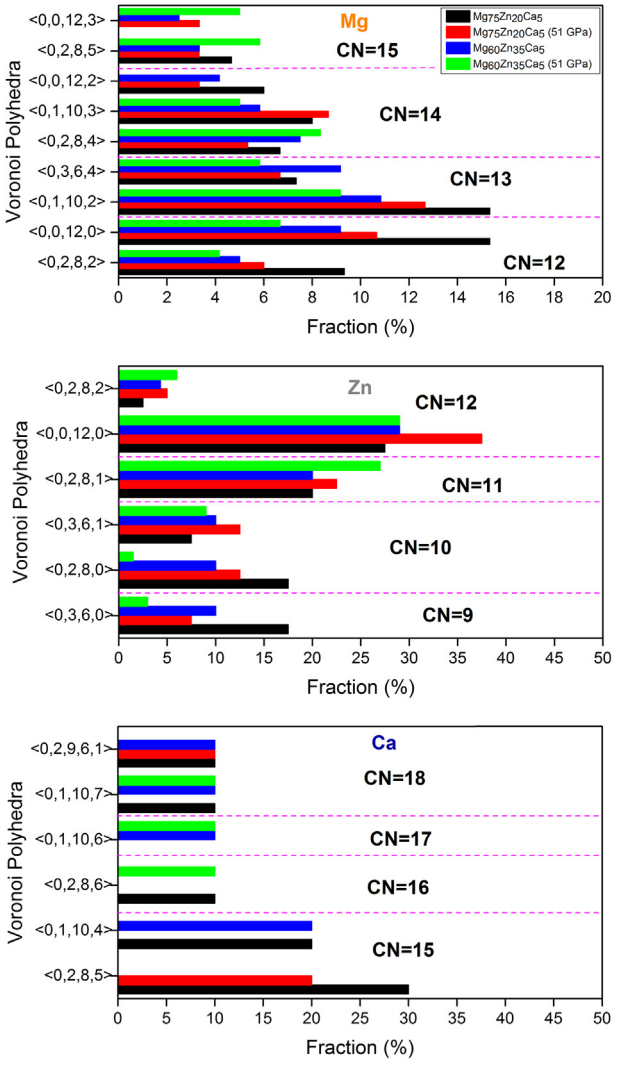

Fig. 7. Distribution of dominant types of Mg-, Zn- and Ca-centered Voronoi polyhedra for all simulated structures.

is located at around 60° for all triplets. Among them, the Mg-Mg-Mg is exactly positioned at 60°, which is assigned to equilateral triangle formations because of the close packing of identical atoms. The first peak of Mg-Zn-Mg and Mg-Ca-Mg are found at 66° and 53°, respectively. The observed shifts in the bond angles could be attributed to atomic radii differences among constituents, viz. $r_{Ca} > r_{Mg} > r_{Zn}$. The second characteristic (broader) peak (β) in the bond angle distribution pattern assigns to interior angle of 108° of a regular pentagon, which is the most common motif in the structure, vide supra. This peak for Mg-Mg-Mg is located at 107° which is slightly different from the ideal angle due to the distortions in the pentagon where one of the five Mg atoms is replaced by Zn and/or Ca. The second peak for Mg-Zn-Mg and Mg-Ca-Mg is located at 120° and 100°, respectively (Fig. 10(a, c, e)). These shifts also can be attributed to atomic radii difference of Mg, Zn and Ca, and thus the shorter Mg-Zn bond and the longer Mg-Ca bond than Mg-Mg bond [29]. Similar trend has been observed in the Zn-Zn-Zn and Zn-Mg-Zn angles (Fig. 10(b, d)). However, as shown in Fig. 10(f), a Zn-Ca-Zn bond angle distribution fluctuates and does not have a regular pattern, which is probably related to low content of Ca in simulations.

The existence and dominating of the main peaks, which are attributed to the close packing and pentagon motifs [29,34], support our previous findings that pentagonal-bipyramid arrangements of atoms are the most common structural configurations in both alloys.

3.6. Chemical short-range order (CSRO)

To explore the chemical short ranger order (CSRO) around the constituents of metallic glasses, the Warren-Cowley parameter, (α_{ij}), which is expressed as follows [41],

$$\alpha_{ij} = 1 - CN_{ij}/(c_j CN_i) \quad (4)$$

was used. In the equation, CN_{ij} is the partial coordination number of atom j around atoms i, c_j is the atomic fraction of the atom j, and CN_i is the total coordination number of atom i. Negative and zero values for α_{ij} denote the existence of CSRO and random solution, respectively. The modified form the Warren-Cowley parameter for a ternary glass is

$$\alpha_{i(jk)} = 1 - (CN_{ij} + CN_{ik})/((c_j + c_k)CN_i) \quad \text{for } i \neq j \neq k \quad (5)$$

Similarly, negative values of $\alpha_{i(j,k)}$ imply the presence of CSRO, but the positive values imply the presence of chemical short range clustering (CSRC) around the atom i. CSRO parameters for binary and ternary alloys are related by,

$$\alpha_{ii} = (1 - 1/c_i)\alpha_{i(jk)} \quad (6)$$

Hence, $\alpha_{ii} < 0$ indicates the CSRC and $\alpha_{ii} > 0$ imply the CSRO. The calculated Warren-Cowley parameters α_{ij} and $\alpha_{i(j,k)}$ are given Tables 3 and 4.

Positive values of α_{MgZn} ascribe the absence of CSRO in the distribution of Zn species around Mg species; negative values of α_{MgCa} indicate the presence of local concentration of Ca atoms around Mg. Also, negative α_{MgMg} values imply the existence of CSRC, namely an increase of local concentration of Mg species around Mg species.

The local distributions around Zn and Ca atoms are found as follows; the positive α_{ZnCa} and α_{ZnMg} values imply a deficit Ca and Mg atoms in Zn-centered clusters while negative α_{ZnZn} values indicate an increase local concentration of Zn atoms in the first coordination shell of Zn. Negative α_{CaMg} values indicate an increase of Mg atoms around Ca whereas positive α_{CaZn} values imply a Zn deficit Ca-centered clusters.

On the other hand, several changes were observed in the CSRO depending on the composition. When Zn content increases from 20% to 35% in the glass, α_{MgCa} value changes from −0.36 to −0.54, while α_{ZnCa} value changes from 0.21 to 0.27. For the former, the negative value increase indicate Ca enrichment around Mg-centered clusters, the latter imply that Ca deficits around Zn-centered clusters. Additionally, α_{ZnZn} value changing from −0.20 to 0.03 indicates an increase of CSRO around Zn, and α_{CaCa} value changing from 0.0 to −0.28 imply an increase of CSRC around Ca (Table 3). However, no noticeable change was observed in α_{MgMg} and α_{MgZn} parameters as a result of the composition change. According to these results, composition change mostly effects on the local environment of Ca and Zn atoms.

Finally, as can be seen from Table 4, $\alpha_{i(j,k)}$ parameters for Ca and Zn centered clusters are almost zero implying a neutral environment around Ca and Zn-centered clusters.

3.7. Local atomic packing efficiency (P)

One of the most important features of BMGs is their higher density than the crystalline phases with the same composition. This high density structure in BMGs is a result of a very effective packing in the amorphous state [34]. The packing efficiency of atoms in the glass is directly linked to the glass formation [42]. To this end, the local atomic

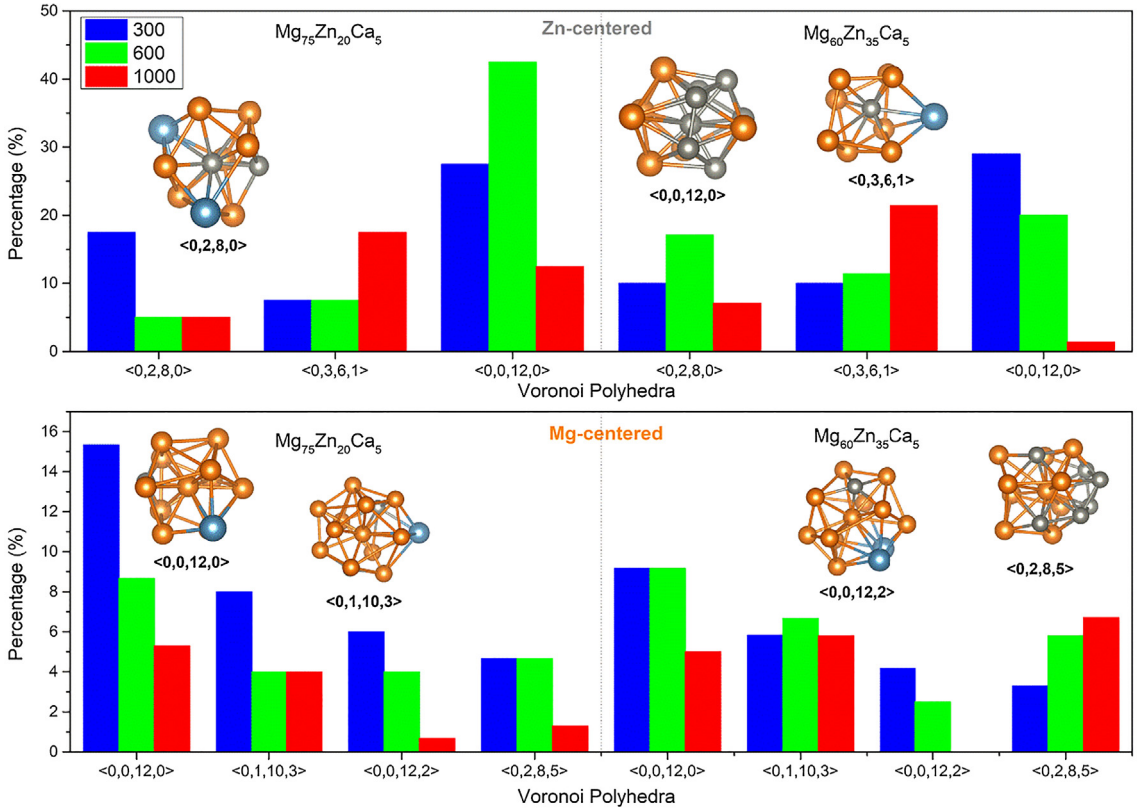

Fig. 8. Distribution of the most altered types of Mg-, Zn- and Ca-centered Voronoi polyhedral as a function of temperature.

packing efficiency (P) is calculated using the method proposed by Miracle [43], with the coordination numbers obtained from Voronoi analysis. For both compositions, P is about 100% for Mg atoms, 100% for Zn atoms and 95% for Ca atoms. These results reveal that all available space in the first coordination shell of Mg and Zn atoms is fully occupied, whereas Ca atoms do not reach the maximum packing efficiency. These values correlate fairly well with the reported P values for Mg-Zn-Ca glasses in the literature [18,21] and further support the idea of high glass forming ability (GFA) this type of BMGs [18].

3.8. High pressure study

We also explore the structural arrangements in both alloys under high hydrostatic pressure and uniaxial stresses (Fig. 11). Note that $Mg_{60}Zn_{35}Ca_5$ is less compressible than $Mg_{75}Zn_{20}Ca_5$. Both partial and total PDFs of BMGs at 51 GPa remarkably move to lower r values, implying a decrease in the average interatomic distances (Figs. 2, 3 and Table 1) [22]. The CNs analysis show that the total CNs of each species increases with the application of pressure, as summarized Table 2. The total CN changes of $Mg_{75}Zn_{20}Ca_5$ under high pressure (at 51GPa) are as follows: from 13.09 to 13.48 (2.9%) for Mg, from 10.65 to 11 (3.2%) for Zn, from 16.00 to 16.80 (5.0%) for Ca. Yet the coordination increases are indeed quite small compared to the densification (about 30%) of these alloys under pressure Additionally, the slight variations in VP distribution were observed under high pressure. For Mg-centered clusters in both alloys at 51 GPa, the fraction of ⟨0,0,12,0⟩, ⟨0,2,8,2⟩ decreases while the percentage of ⟨0,1,10,3⟩, ⟨0,2,8,4⟩ increases. This can be explained as follows: As the atoms more approach each other under high pressure, the coordination number increases. Already, the CN analysis confirms this hypothesis (Fig. 7). For high pressurized form of both compositions, 1431, 1541 and 1551 type of BPs are in majority, as shown in Fig. 9(a). Remarkably, with increasing pressure, the percentage of 1551, 1441 and 1661 increases while that of 1421, 1422, 1431 and 1541 decreases. A diminishing in fcc/hcp ordering and an enlargement in ideal icosahedral ordering specify more disordered structures in these alloys. The Warren-Cowley parameters for metallic glasses and their high density forms are almost same, i.e. pressure at 51GPa did not significantly affect the local chemical environment of these glasses (Tables 3 and 4). In addition, the behavior of both glasses under uniaxial stresses was also studied. As can be seen from Fig. 12, both materials exhibit structural anisotropy as in the most disordered system [35]. According to the results, both compositions show structural failure between 6 and 8 GPa and the highest axial strength was found in y-direction.

3.9. Mechanical properties

As already mentioned, Mg-based metallic glasses are the most promising candidate for biodegradable implant materials. To this end, it is very important to determine their mechanical properties. Thus, some mechanical properties for both compositions were examined. To calculate the bulk modulus (B), a measure of compressibility of the material under hydrostatic pressure, metallic glasses were relaxed at different pressures (between −5 GPa and 7 GPa) using conjugate gradient variable cell optimization technique, and the energy-volume values were fitted to the third order Birch-Murnaghan equation of state (Eq. (7)).

$$E(V) = E_0 + \frac{9V_0B_0}{16}\left\{\left[\left(\frac{V_0}{V}\right)^{\frac{2}{3}}-1\right]^3 B_0' + \left[\left(\frac{V_0}{V}\right)^{\frac{2}{3}}-1\right]^2\left[6-4\left(\frac{V_0}{V}\right)^{\frac{2}{3}}\right]\right\} \quad (7)$$

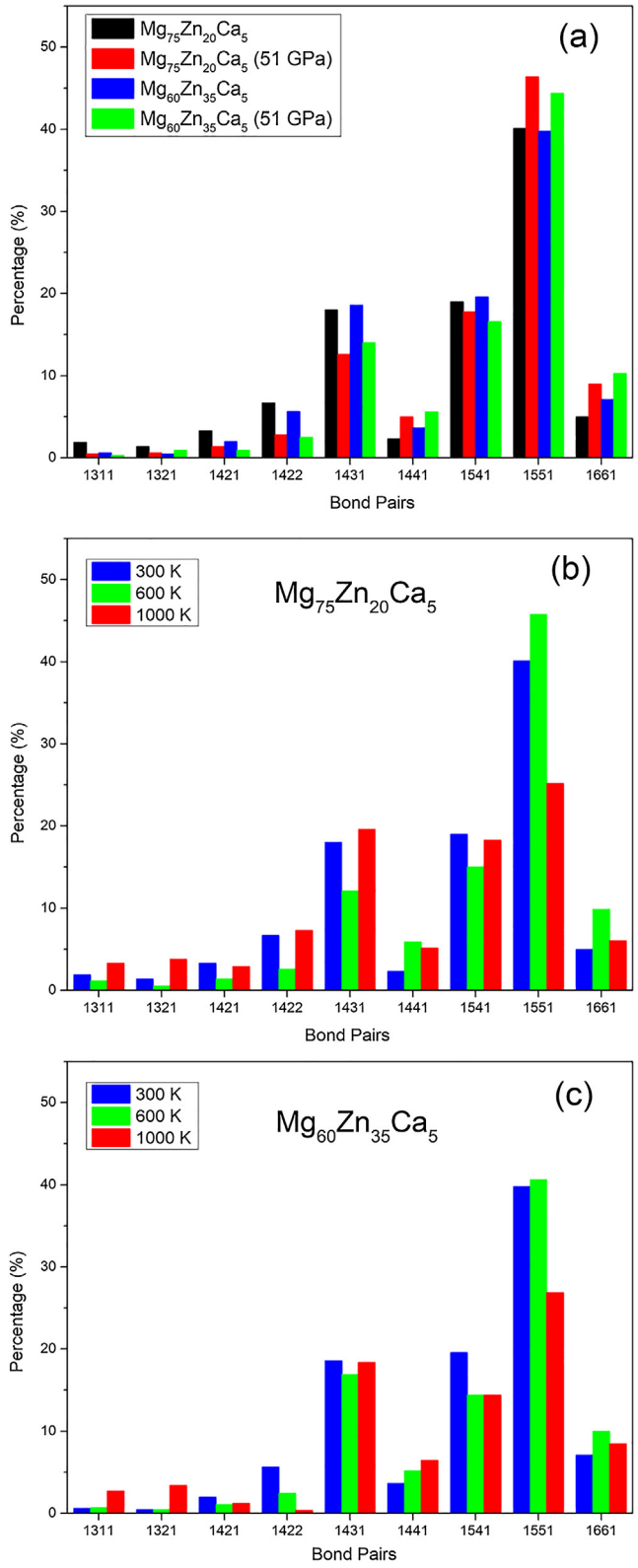

Fig. 9. (a) Honeycutt-Andersen BP distributions for all simulated structures. (b-c) BP distributions for each composition.

In this equation, E_0 and V_0 correspond to the energy and volumes in the equilibrium state, respectively. From the fitted data, the equilibrium volumes of $Mg_{75}Zn_{20}Ca_5$ and $Mg_{60}Zn_{35}Ca_5$ glasses were estimated 21.9 and 20.8 Å^3/atom, respectively (Fig. 13). The more dense structure of Zn-rich metallic glass can be attributed to the fact that Zn atom is heavier than Mg atom and the increased coordination number with the increasing of Zn content in the glasses. The bulk moduli (B) of $Mg_{75z}n_{20}Ca_5$ and $Mg_{60}Zn_{35}Ca_5$ glasses were determined to be 43.2 and 46.8 GPa, respectively.

Another important parameter used to describe the mechanical properties of a material in the elastic region is the Poisson's ratio, which is defined as the ratio of transverse contractional strain to longitudinal extensional strain. When the material is compressed along the axial direction, the Poisson's ratio,

$$\nu = -\frac{\Delta\varepsilon_{trans}}{\Delta\varepsilon_{axial}} \tag{8}$$

where ε_{trans} and ε_{axial} are transverse and axial strains, respectively. During the compression process, axial strain value is negative while transverse strain is positive. To calculate the Poisson's ratio, the uni-axial stresses (σ_x σ_y σ_z) were separately applied to the simulation box and the system was relaxed under these stresses. Two Poisson's ratios were obtained for each axial stress and six in total. The mean Poison's ratio estimated from these six values is 0.359 ± 0.03 (max. 0.379 and min. 0.306) for $Mg_{75}Zn_{20}Ca_5$ and 0.291 ± 0.02 (max. 0.299 and min. 0.257) for and $Mg_{60}Zn_{35}Ca_5$. Taking into account the errors arising from calculations, the values we obtain are quite consistent with the literature, as can be seen from Table 5.

$$E = 3B(1-2\nu) \tag{9}$$

The elastic (or Young's) modulus is a measure of the resistance of the material to changes in size under compression or tension. Stiff materials have a high elastic modulus (small changes in dimensions under low loads), while flexible materials have a low elastic modulus (considerable change in size even under low loads.) Indeed, the elastic constants defining a solid are related to each other and one can be expressed in terms of another. Elastic modulus depends on both bulk modulus and Poisson ratio as follows

The elastic modulus calculated for $Mg_{75}Zn_{20}Ca_5$ and $Mg_{60}Zn_{35}Ca_5$ are 36.55 and 58.69 GPa, respectively. Obviously, the stiffness of the material increases with the increase of Zn content in the glasses the most probably due to an increase in CN and closer packing of atoms.

The shear modulus is another measure of the rigidity of the solid materials. Materials with larger shear modulus are more rigid, whereas materials have low shear modulus flexible. Shear modulus in terms of elastic modulus and Poisson's ratio:

$$G = \frac{E}{2(1+\nu)} \tag{10}$$

The calculated shear modulus from this expression is found to be 13.45 and 22.73 GPa for $Mg_{75}Zn_{20}Ca5$ and $Mg_{60}Zn_{35}Ca_5$, respectively.

Lastly, the Vickers hardness, defined as indentation or penetration resistance of a material, were calculated. In the literature, Teter shows that there is a linear correlation between hardness and shear modulus of a material, and he proves that it can also be used for BMGs [44,45]. Vickers hardness defined by Teter [44]:

$$H_v = 0.151G \tag{11}$$

The calculated hardness values for $Mg_{75}Zn_{20}Ca_5$ and $Mg_{60}Zn_{35}Ca_5$ are 2.03 and 3.43 GPa, respectively.

Table 5 summarizes the elastic constants obtained in this work as well as the data reported in the literature on Mg-based metallic glasses. Obviously, the calculated elastic constant in this study are similar to those in the literature [9,21,46]; this also supports that our calculations are reliable. According to the method proposed by Lewandowski [47], it is possible determine whether a metallic glass is brittle or ductile using elastic constants. In this method, metallic glasses with G/

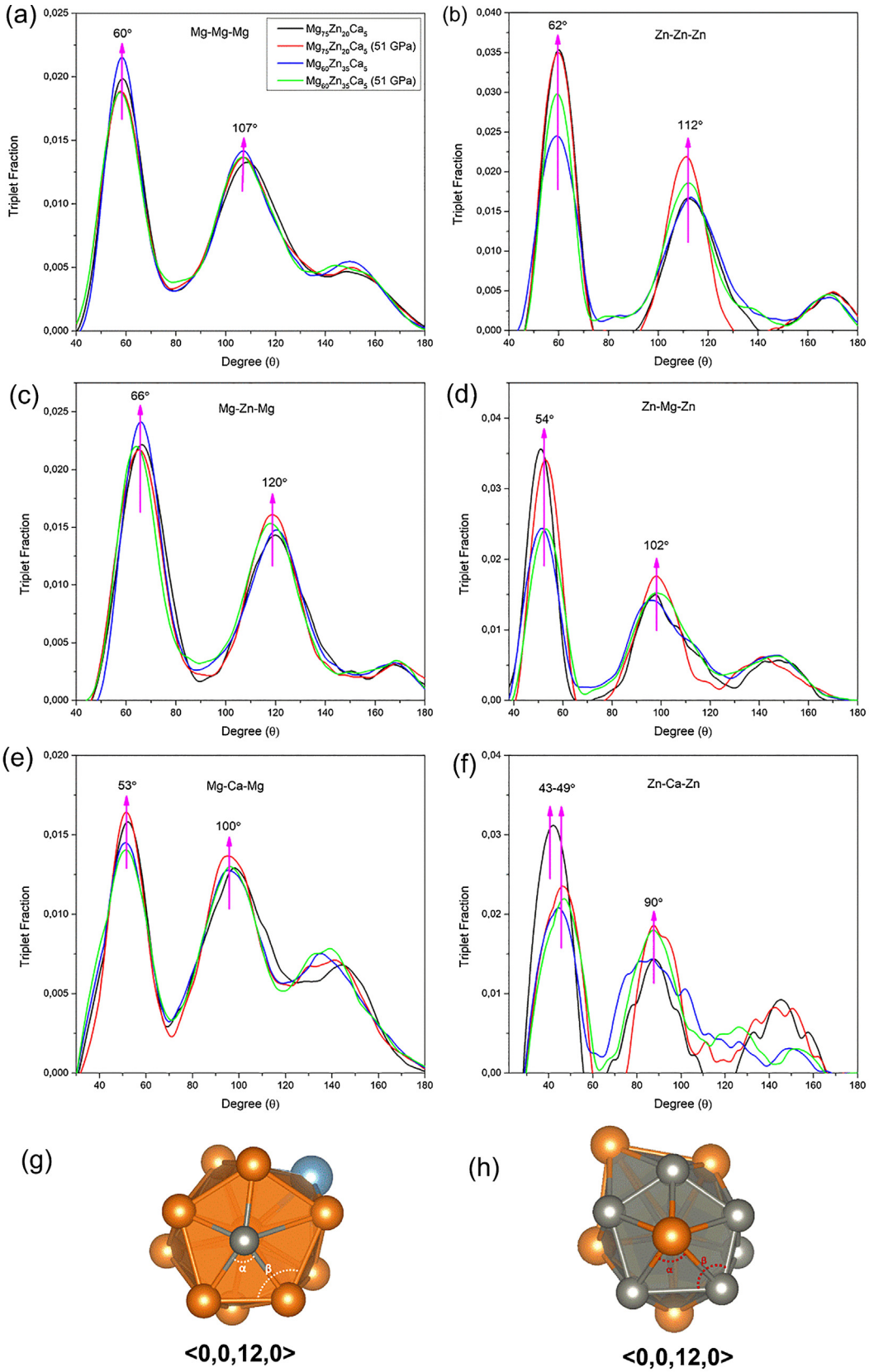

Fig. 10. (a–f) Bond angle distributions for Mg-X-Mg and Zn-X-Zn triplets, (g) Mg-centered ⟨0,0,12,0⟩ VP (h) Zn-centered ⟨0,0,12,0⟩ VP (VPs were picked from the relaxed simulation box (0 K and 0 GPa) with $Mg_{75}Zn_{20}Ca_5$ composition.)

Table 3
Chemical short range order parameters (a_{ij}) for Mg-, Zn-, and Ca-centered clusters.

α_{ij}	Mg-Mg	Mg-Zn	Mg-Ca	Zn-Mg	Zn-Zn	Zn-Ca	Ca-Mg	Ca-Zn	Ca-Ca
$Mg_{75}Zn_{20}Ca_5$	−0.03	0.21	−0.36	0.04	−0.20	0.21	−0.13	0.47	0.00
$Mg_{75}Zn_{20}Ca_5$ (51 GPa)	−0.03	0.21	−0.39	0.03	−0.16	0.15	−0.12	0.43	0.02
$Mg_{60}Zn_{35}Ca_5$	−0.07	0.20	−0.54	0.04	−0.03	0.27	−0.24	0.53	−0.28
$Mg_{60}Zn_{35}Ca_5$ (51 GPa)	−0.06	0.16	−0.47	0.03	−0.01	0.25	−0.26	0.47	−0.21

Table 4
Chemical short range order parameters ($a_{i(jk)}$) for Mg-, Zn-, and Ca-centered clusters.

$\alpha_{i(jk)}$	Mg	Zn	Ca
$Mg_{75}Zn_{20}Ca_5$	0.10	0.05	0.00
$Mg_{75}Zn_{20}Ca_5$ (51 GPa)	0.09	0.04	0.00
$Mg_{60}Zn_{35}Ca_5$	0.10	0.02	0.05
$Mg_{60}Zn_{35}Ca_5$ (51 GPa)	0.08	0.00	0.01

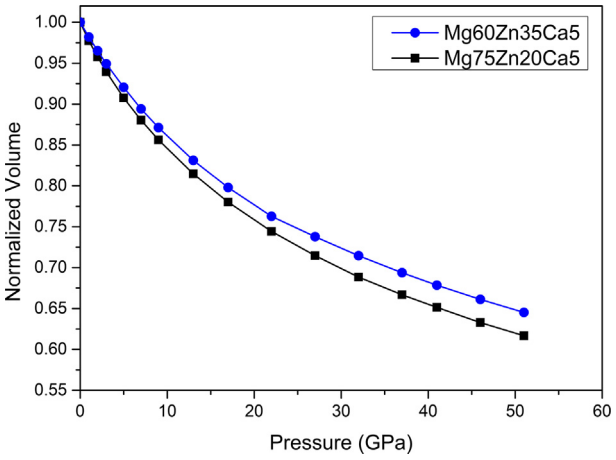

Fig. 11. Volume change as a function of hydrostatic pressure in both composition BMGs.

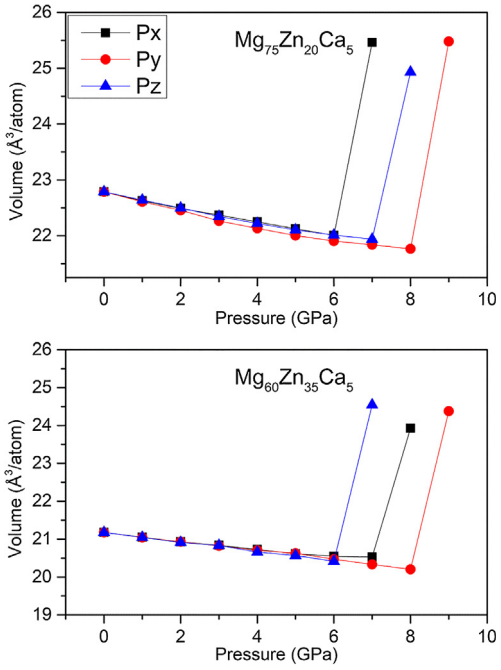

Fig. 12. Volume change as a function of axial pressure in both composition BMGs.

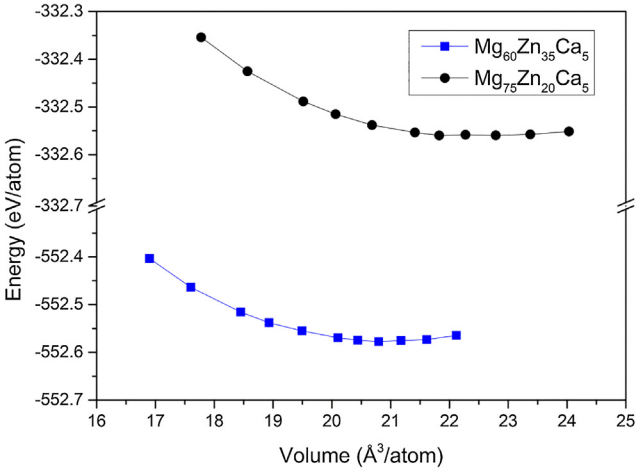

Fig. 13. Energy-volume relation for both composition BMGs.

B > 0.41–0.43 (or/and with ν < 0.31–0.32) are defined as brittle materials. Obviously, while $Mg_{75}Zn_{20}Ca_5$ is in the ductile region, $Mg_{60}Zn_{35}Ca_5$ is a brittle material. This can be attributed to an increase in CN and therefore a tighter (closer) packing in the glasses due to increase of smaller size Zn atoms, as shown by structural analyzes in previous sections of this work.

4. Conclusions

To sum up, we have performed AIMD simulations of two different compositions of Mg-Zn-Ca metallic glasses. These alloys show the following structural and mechanical characteristics:

i. As the content of Zn increases in the alloy, it has been observed that the shifts to smaller *r* values in total PDF peaks and the increase in the coordination number for each constituent in the alloy. This can be explained by the atomic size difference between Mg and Zn atoms. The incorporation of relatively smaller size Zn atoms into the alloy results in a decrease in average interatomic distances, especially in Mg-Ca, Zn-Ca, and Zn-Mg, and also more dense atomic packing.
ii. The Voronoi tessellation and CN analyzes reveal that Zn atoms mostly tend to coordinate with Mg atoms.
iii. The icosahedral ordering is favorable in Zn-centered clusters according to the Voronoi analysis.
iv. The Honeycutt-Andersen bond pair analysis show a diminishing in fcc/hcp ordering and an enlargement in icosahedral ordering, indicating more disordered structures in both alloys.
v. The Voronoi, bond pair and bond-angle distribution analyzes prove the dominance of 5-fold atomic arrangements in the alloys.
vi. The maximum local atomic packing ability for both alloy support the high glass forming ability of Mg-Zn-Ca alloys.
vii. The most striking results to emerge from the mechanical properties calculations is that an increase of Zn (≥30%) content in the alloy results in embrittlement in the alloys. This is a very remarkable observation for designing this type of metallic glass because the slower corrosion rates can only be achievable in Mg-Zn-Ca metallic

Table 5
The calculated elastic constants for simulated compositions (B = Bulk modulus, v = Poisson' ratio, E = theYoung' modulus, G = shear modulus, Hv = Vickers hardness, B/G, ρ = density).

Composition	B (GPa)	ν	E (GPa)	G (GPa)	G/B	H_v (GPa)	ρ(g/cm^3)	Ref.
$Mg_{75}Zn_{20}Ca_5$	43.2	0.359 (± 0.03)	36.55	13.45	0.31	2.03	2.48	This work
$Mg_{60}Zn_{35}Ca_5$	46.8	0.291 (± 0.02)	58.69	22.73	0.48	3.43	3.10	This work
$Mg_{65}Cu_{25}Tb_{10}$	53.2	0.309	55.1	19.6	0.37	2.83	–	[46]
$Mg_{65}Cu_{25}Gd_{10}$	45.1	0.313	50.6	19.3	0.43	–	–	[46]
$Mg_{72}Zn_{24}Ca_4$	44.0	0.359	–	13.69	0.31	–	2.62	[21]
$Mg_{62}Zn_{32}Ca_6$	43.9	0.286	–	21.93	0.50	–	2.92	[21]
$Mg_{64}Ni_{21}Nd_{15}$	44.8	0.324	47.4	17.9	0.40	–	3.70	[6]
$Mg_{57}Cu_{34}Nd_9$	50.7	0.322	54.2	20.5	0.40	–	4.1	[5]
$Mg_{66}Zn_{30}Ca_4$	40.1	0.299	48.4	18.65	0.47	–	2.92	[9]
Human Bone	–	0.14–0.32	12–23	7.9–13.2	–		1.1–1.80	[48–50]

glasses with at least 28% Zn content. In the view of such findings, an improvement in corrosion resistance results in a diminishment in malleability.

Acknowledgements

This work was supported by the Abdullah Gül University Support Foundation. The calculations were run on TÜBİTAK ULAKBİM, High Performance and Grid Computing Center (TRUBA resources).

References

[1] A.L. Greer, Science 267 (1995) 1947–1953.
[2] A. Inoue, Acta Mater. 48 (2000) 279–306.
[3] J. Schroers, Phys. Today 66 (2013) 32–37.
[4] A.L. Greer, Mater. Today 12 (2009) 14–22.
[5] L.L. Shi, J. Xu, J. Non-Cryst Solids 357 (2011) 2926–2933.
[6] S.G. Wang, L.L. Shi, J. Xu, J. Mater. Res. 26 (2011) 923–933.
[7] B. Zberg, P.J. Uggowitzer, J.F. Loffler, Nat. Mater. 8 (2009) 887–891.
[8] X.N. Gu, Y.F. Zheng, S.P. Zhong, T.F. Xi, J.Q. Wang, W.H. Wang, Biomaterials 31 (2010) 1093–1103.
[9] Y.Y. Zhao, X. Zhao, J. Alloy Compd. 515 (2012) 154–160.
[10] D.M. Miskovic, K. Pohl, N. Birbilis, K.J. Laws, M. Ferry, J. Mater. Chem. B 4 (2016) 2679–2690.
[11] J.K. Christie, Phys. Chem. Chem. Phys. 17 (2015) 12894–12898.
[12] Y.B. Wang, X.H. Xie, H.F. Li, X.L. Wang, M.Z. Zhao, E.W. Zhang, Y.J. Bai, Y.F. Zheng, L. Qin, Acta Biomater. 7 (2011) 3196–3208.
[13] P.C. Wong, T.H. Lee, P.H. Tsai, C.K. Cheng, C. Li, J.S.C. Jang, J.C. Huang, Metals-Basel 6 (2016).
[14] M.S. Dambatta, S. Izman, B. Yahaya, J.Y. Lim, D. Kurniawan, J. Non-Cryst Solids 426 (2015) 110–115.
[15] Y.C. Liang, R.S. Liu, Q. Xie, Z.A. Tian, Y.F. Mo, H.T. Zhang, H.R. Liu, Z.Y. Hou, L.L. Zhou, P. Peng, Sci. Rep.-Uk 7 (2017) 1–11.
[16] M. Durandurdu, J. Chem. Phys. 137 (2012).
[17] S.P. Ju, H.H. Huang, J.C.C. Huang, J. Non-Cryst Solids 388 (2014) 23–31.
[18] A. Gulenko, L.F. Chungong, J.H. Gao, I. Todd, A.C. Hannon, R.A. Martin, J.K. Christie, Phys. Chem. Chem. Phys. 19 (2017) 8504–8515.
[19] G. Kresse, J. Non-Cryst Solids 193 (1995) 222–229.
[20] Y.F. Zhao, D.Y. Lin, X.H. Chen, Z.K. Liu, X.D. Hui, Acta Mater. 67 (2014) 266–277.
[21] R. Mahjoub, K.J. Laws, J.P. Scicluna, J.E. Daniels, M. Ferry, Comput. Mater. Sci. 96 (2015) 246–255.
[22] S.N. Li, J.B. Liu, J.H. Li, J. Wang, B.X. Liu, J. Phys. Chem. B 119 (2015) 3608–3618.
[23] J.M. Soler, E. Artacho, J.D. Gale, A. Garcia, J. Junquera, P. Ordejon, D. Sanchez-Portal, J. Phys.-Condens. Mater. 14 (2002) 2745–2779.
[24] N. Troullier, J.L. Martins, Phys. Rev. B 43 (1991) 1993–2006.
[25] J.P. Perdew, K. Burke, M. Ernzerhof, Phys. Rev. Lett. 77 (1996) 3865–3868.
[26] K. Momma, F. Izumi, J. Appl. Crystallogr. 44 (2011) 1272–1276.
[27] Y.Q. Cheng, E. Ma, H.W. Sheng, Phys. Rev. Lett. 102 (2009).
[28] P. Andonov, P. Chieux, J. Non-Cryst Solids 93 (1987) 331–349.
[29] O.N. Senkov, D.B. Miracle, E.R. Barney, A.C. Hannon, Y.Q. Cheng, E. Ma, Phys. Rev. B 82 (2010).
[30] T. Fukunaga, K. Itoh, T. Otomo, K. Mori, M. Sugiyama, H. Kato, M. Hasegawa, A. Hirata, Y. Hirotsu, A.C. Hannon, Intermetallics 14 (2006) 893–897.
[31] J. Saida, K. Itoh, S. Sato, M. Imafuku, T. Sanada, A. Inoue, J. Phys.-Condens. Mater. 21 (2009).
[32] H.W. Sheng, W.K. Luo, F.M. Alamgir, J.M. Bai, E. Ma, Nature 439 (2006) 419–425.
[33] S.P. Pan, S.D. Feng, J.W. Qiao, W.M. Wang, J.Y. Qin, Sci. Rep.-Uk 5 (2015).
[34] D.B. Miracle, Nat. Mater. 3 (2004) 697–702.
[35] Y.Q. Cheng, E. Ma, Prog. Mater Sci. 56 (2011) 379–473.
[36] P.J. Steinhardt, D.R. Nelson, M. Ronchetti, Phys. Rev. Lett. 47 (1981) 1297–1300.
[37] J.D. Honeycutt, H.C. Andersen, J. Phys. Chem.-Us 91 (1987) 4950–4963.
[38] M. Durandurdu, Comput. Mater. Sci. 65 (2012) 44–47.
[39] H.J. Lee, T. Cagin, W.L. Johnson, W.A. Goddard, J. Chem. Phys. 119 (2003) 9858–9870.
[40] J. Hafner, J. Phys.-Paris 46 (1985) 69–78.
[41] O.N. Senkov, Y.Q. Cheng, D.B. Miracle, E.R. Barney, A.C. Hannon, C.F. Woodward, J. Appl. Phys. 111 (2012).
[42] D.B. Miracle, W.S. Sanders, O.N. Senkov, Phil. Mag. 83 (2003) 2409–2428.
[43] D.B. Miracle, J. Non-Cryst Solids 342 (2004) 89–96.
[44] D.M. Teter, Mrs Bull. 23 (1998) 22–27.
[45] X.Q. Chen, H.Y. Niu, D.Z. Li, Y.Y. Li, Intermetallics 19 (2011) 1275–1281.
[46] W.H. Wang, J. Appl. Phys. 99 (2006).
[47] J.J. Lewandowski, W.H. Wang, A.L. Greer, Phil. Mag. Lett 85 (2005) 77–87.
[48] P.C. Dechow, G.A. Nail, C.L. Schwartzdabney, R.B. Ashman, Am. J. Phys. Anthropol. 90 (1993) 291–306.
[49] M.J. Mirzaali, J.J. Schwiedrzik, S. Thaiwichai, J.P. Best, J. Michler, P.K. Zysset, U. Wolfram, Bone 93 (2016) 196–211.
[50] C.S. Jorgensen, T. Kundu, J. Orthopaed. Res. 20 (2002) 151–158.